*Progress In Electromagnetics Research Letters, Vol. 110, 29–36, 2023*

# A Terahertz Low Scan Loss High Gain Beam Steering Transmitarray

**Guang Liu[1, *], Zhenzhan Wang[1], Haowen Xu[1, 2], Min Yi[1], and Haotian Zhu[1]**

**Abstract**—This paper presents a terahertz high gain beam steering transmitarray antenna (BSTA) working at 340 GHz. Substrateless double hexagon ring slots unit-cells which present low loss characteristics at THz band are used to constitute the layout of THz BSTA. To improve the beam steering performance, bifocal technique is used to design the layout of BSTA. Because the fabrication risk of the THz BSTA prototype increases a lot as the aperture dimension is enlarged, four inch silicon wafer is chosen after weighting the risk and gain of the BSTA. Micromachining process is used to fabricate the large aperture THz BSTA to ensure the machining accuracy of the unit-cells. The measured results of the prototype show that the THz BSTA could realize $-15^\circ \sim 15^\circ$ range beam scanning with gain $> 38.3$ dB, scanning loss $< 1.2$ dB, and side lobe level $< -17.8$ dB, by moving the feed along the focal plane of the BSTA.

## 1. INTRODUCTION

Deep space exploration at terahertz band has attracted more and more attention these years [1, 2]. The working frequencies of terahertz limb sounder cover frequencies from 118 GHz to 2.5 THz, and many key spectrum lines of the molecules such as $O_3$, HCl, $H_2O$, $HNO_3$, $CH_3CN$, $N_2O$, ClO, CO, HCN, OH, $SO_2$, and ice water content (IWC) of clouds could be observed at the frequency band [3]. In terahertz limb sounder system, beam steering antennas that could flexibly change the beam to the specified direction are usually used to realize vertically layered atmospheric detection, which could save volume and weight compared to traditional mechanical scanning antennas.

Transmitarray antennas (TAs) are a kind of lens antenna with flat structure, which combines the optical theory and array technique. The transmission unit-cells periodically distributed on the panel of TA could compensate the spherical wave front phase to plane wave radiated from the feed, so as to realize high gain beam at specific direction [4, 5]. TAs are very good candidates for high speed moving platforms such as vehicles, unmanned aerial vehicles (UAVs), and small satellites because their flat panel profile and light weight features [6].

Because the penetration ability of terahertz wave is weak, the reflection and transmission loss on the surface of and inside the substrate will greatly affect the performances of THz TA [7]. Standard printed-circuit-board (PCB) process has been used to fabricate THz TAs working at 250 GHz and 0.3 THz in [8–10], respectively. Receiving/transmitting elements based on low-temperature co-fired ceramic (LTCC) technology has also been used to fabricate a high gain and high aperture efficiency THz TA working at 140 GHz [11]. Three metal layers receiving/transmitting elements with more than 30% fractional band based on PCB technology were used to fabricate a wideband high gain TA working at D-band ($120 \sim 170$ GHz) [12]. To eliminate dielectric loss induced by substrate, a substrateless THz TA working at 340 GHz was fabricated by two inch silicon wafer micromaching technology [13]. Perfect transmission and complete phase control have been realized by accurate model of the unit-cell

*Received 28 January 2023, Accepted 10 March 2023, Scheduled 1 April 2023*

* Corresponding author: Guang Liu (liuguang@mirslab.cn).

[1] Key Laboratory of Microwave Remote Sensing, National Space Science Center, Chinese Academy of Sciences, Beijing 100190, China. [2] University of Chinese Academy of Sciences, Beijing 100190, China.

anisotropic behavior in [14], and a three layer TA without any vias working at 300 GHz was fabricated by PCB process, which could reach 36.5% aperture efficiency and 25.1% of 3-dB bandwidth.

Mechanically moving the feed along the focal plane of passive TA is a good solution to realize beam steering, which avoids using solid state switches and corresponding DC bias controlling lines in reconfigurable TA (RTA) [15] and reconfigurable reflectarray (RRA) [16], but the scanning loss could reach 5 dB for $\pm 30^\circ$ steering range because of the higher spillover loss and phase aberration loss as the feed moving further off the TA's focus [17]. The scanning loss of steering beams could be reduced to 2.8 dB for wide angular scanning range of $50^\circ$ by introducing bifocal Gaussian weight functions and expanding the transverse aperture of TA [18, 19].

A novel terahertz high gain beam steering TA (BSTA) centered working at 340 GHz is demonstrated in this paper. Substrateless double hexagonal ring slots unit-cell presented in [20] which expresses low loss performances at terahertz band is used to constitute the layout of THz BSTA. Improved bifocal theory is used to design the phase distribution of BSTA to promote the phase compensation effect as the feed offset the center focus of BSTA. A prototype is manufactured by four inch silicon wafer micromachining process whose area is almost four times of the two inch THz substrateless TA shown in [13]. The fracture risk of the metal unit-cell layer increases unpredictably as the diameter increases, and improved manufacture process is proposed in the paper to prevent the risk. Two optical theodolites are used to calibrate the position relationship between the feed and THz BSTA in measurement. The measured results of the prototype indicate that high gain, low side lobe level, and quite low scanning loss are reached by the steering beams.

## 2. DETAILED DESIGN OF THZ BEAM STEERING TRANSMITARRAY

### 2.1. THz Bifocal BSTA Design

The proposed architecture figure of THz BSTA is shown in Fig. 1. The aperture dimensions of BSTA are $D_x \times D_y$, and $D_y$ is larger than $D_x$ to decrease spillover loss as the feed deviates from the central focal point of the TA. The THz BSTA has two focal points, $Fp_1$ and $Fp_2$, located at $(x, y_1, -F)$ and $(x, y_2, -F)$, respectively. $F$ is the focal length of the THz TA. A THz pyramidal horn is used to illuminate the BSTA, and the main beam direction could steer from $\theta_1$ to $\theta_2$ as the horn moving from $f_1$ to $f_2$.

To improve radiation performances of scanning beams as the feed moving along the focal line of BSTA, bifocal theory is introduced to design the proposed THz TA, and the bifocal TA phase distribution design formulas are shown as follows [19].

$$\phi_{bifocal} = \frac{w_1 \times \phi_1 + w_2 \times \phi_2}{w_1 + w_2} \tag{1}$$

where $\phi_i$ $(i = 1, 2)$ are unifocal phase distributions as the focal points are located at $f_1$ and $f_2$, respectively,

$$\phi_i = k_0 \left( \sqrt{x^2 + (y - y_i)^2 + F^2} - y_i \sin\theta_i \right) \tag{2}$$

$w_1$ and $w_2$ are exponential weight coefficients according to illuminating edge taper of the feed,

$$w_i = e^{-\frac{x^2 + (y - y_i)^2}{2\sigma^2}} \tag{3}$$

$\sigma$ is the weight parameter and expressed as

$$\sigma^2 = \frac{D_x^2}{8\tau \ln 10} \tag{4}$$

where $\tau$ is calculated by illuminating edge taper $T_e$

$$\tau = -\frac{T_e}{20} \tag{5}$$

The corresponding design parameters are shown as follows: $D_x = 70$ mm, $D_y = 89$ mm, $\tau = 0.7$ (corresponding to illuminating edge taper of $T_e = -14$ dB), $\sigma = 13.8$, $y_1 = -9.38$ mm, $\theta_1 = 15^\circ$,

$y_2 = 9.38\,\text{mm}$, and $\theta_2 = -15°$. $F = 35\,\text{mm}$ corresponding to $F/D_x = 0.5$ is chosen base on our previous design experiences in [21]. The periodic size of unit-cell is $P = 0.57\lambda_0 = 0.5\,\text{mm}$, and $\lambda_0$ is the free-space wavelength at the centered working frequency of 340 GHz. The layout of the BSTA is constituted by $140 \times 178$ unit-cells arranged in an elliptical frame, as shown in Fig. 1. According to the bifocal TA phase design function (1), the computed phase distribution of THz bifocal BSTA is shown in Fig. 2.

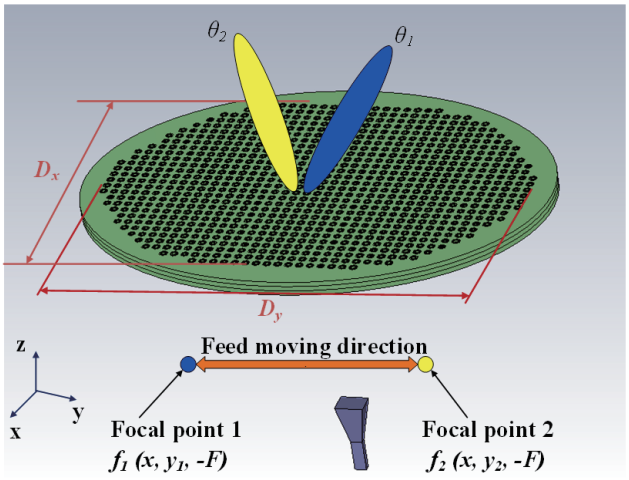


**Figure 1.** Architecture figure of THz BSTA.

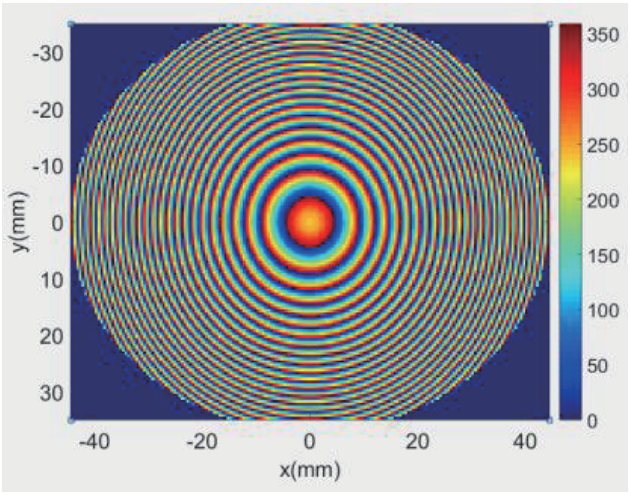


**Figure 2.** Computed transmission phase distribution of THz bifocal BSTA.

The substrateless four layers double hexagonal ring slots unit-cell which shows low transmission loss better than $-1$ dB at 340 GHz is used to constitute the layout of THz bifocal TA, as shown in Fig. 3. The unit-cell contains four metal layers with the thickness of $T = 0.01\,\text{mm}$, and there are three identical air gaps with a height of $H = 0.21\,\text{mm}$ between adjacent metal layers, as shown in Fig. 3(b). There are two concentric hexagonal ring slots on each metal layer. The radius of the inner hexagonal ring is $r$. The width of hexagonal ring slot and gap between two slots are set $w = 0.05\,\text{mm}$ and $g = 0.05\,\text{mm}$, respectively. On the left and right sides of the unit-cell, there are two symmetrical 30° triangular notches, as show in Fig. 3(a).

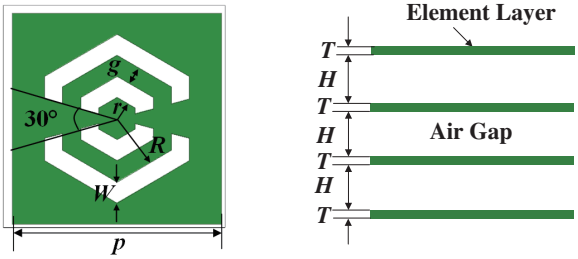


(a) (b)

**Figure 3.** Substrateless double hexagonal ring slots unit-cell. (a) Top view. (b) Side view.

Figure 4 presents the simulated transmission coefficients vs. frequency of the different unit-cells with 0°, 90°, 180°, and 270° states (corresponding to $r = 81\,\mu\text{m}$, $70\,\mu\text{m}$, $60\,\mu\text{m}$ and $86\,\mu\text{m}$, respectively) at 340 GHz. The results show that the transmission magnitudes are better than $-3$ dB between 313 GHz and 344 GHz for all the unit-cells, which represents that the $-3$ dB fractional bandwidth is 9.1% around 340 GHz. In the whole bandwidth, the transmission phase curves are quasi-linear and parallel. A THz pyramid horn has been used as the feed of THz BSTA. The gain of 12.8 dBi and illuminating edge taper of $-14$ dB are offered by the THz pyramid horn at 340 GHz.

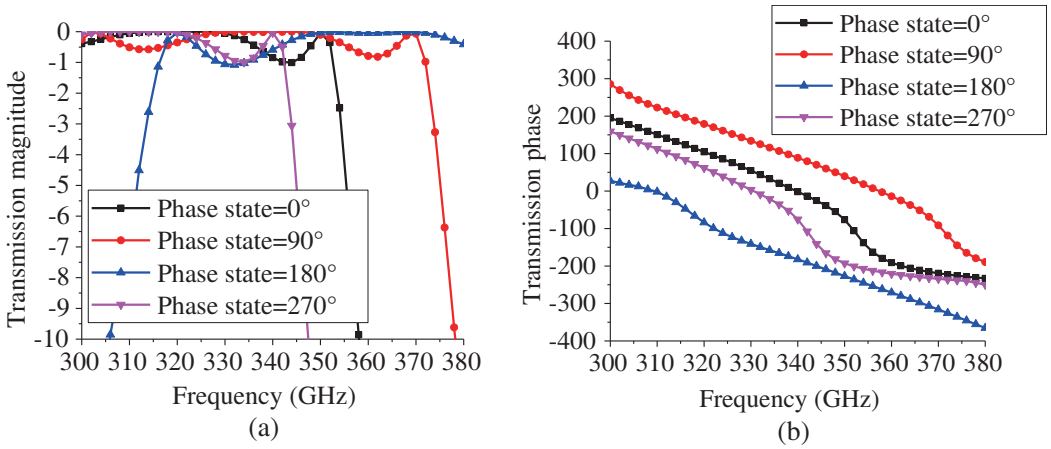


**Figure 4.** Transmission (a) Magnitude and (b) phase of the unit-cells with 0°, 90°, 180° and 270° state at 340 GHz.

## 3. FABRICATION OF THE THZ BSTA

The microfabrication process presented in [13] was used to manufacture the four inch diameter substrateless THz TA. In order to prevent fracture of the electroplated metal layer, which without silicon substrate support in the middle section of the BSTA, 3 μm nickel layer was electroplated in the middle of the copper layer to improve toughness of the electroplated metal layer, as shown in Fig. 5. Two pairs of high precision vernier caliper unit-cells are used to realize high precision alignment between adjacent layers for transverse and longitudinal directions [22].

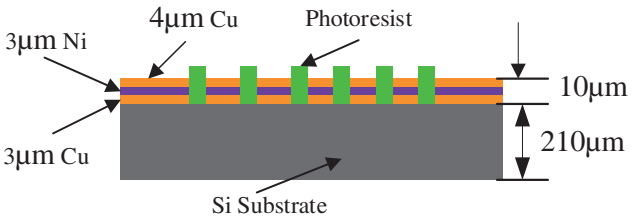


**Figure 5.** Electroplated metal layers on the Si substrate.

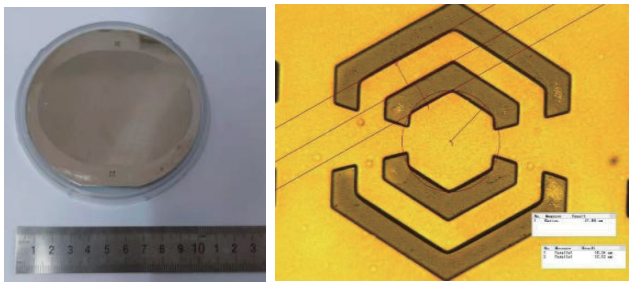


**Figure 6.** (a) Photo of fabricated THz BSTA prototype and (b) optical microscope image of fabricated double hexagonal ring slots unit-cell.

A photo of the fabricated THz BSTA prototype is shown in Fig. 6(a). The optical microscope image of fabricated double hexagonal ring slots unit-cell is shown in Fig. 6(b), and the unit-cells are completely processed according to the design drawing. The measured dimension errors of fabricated unit-cells are less than 1 μm, which have very little impacts on the transmission performances.

## 4. EXPERIMENTAL RESULTS

The far-field radiation patterns of the THz BSTA were measured by NSI Model 905 V high frequency (40–500 GHz) planar near-field system. Two optical theodolites are used to calibrate the position relationship between the feed and THz BSTA, as shown in Fig. 7. A high precision three-dimensional optical displacement platform was used to adjust feed's position precisely. A measurement photo of the

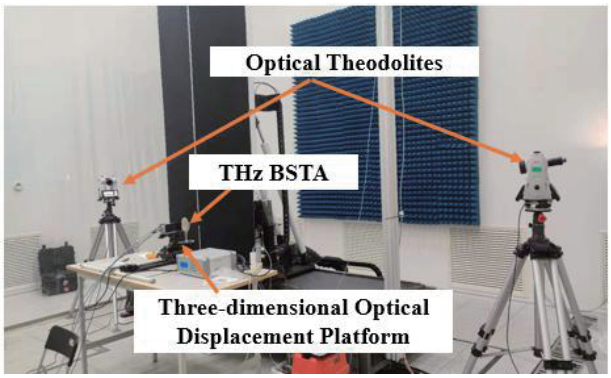


**Figure 7.** Position relationship calibration between the feed and THz BSTA.

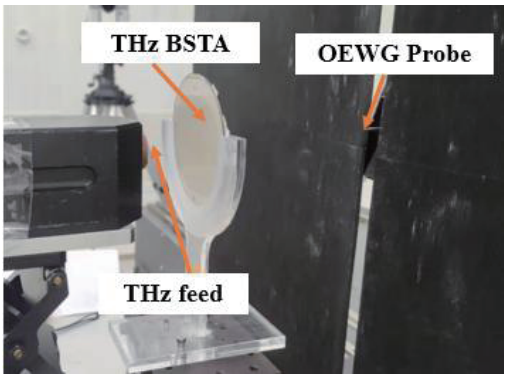


**Figure 8.** THz BSTA measured by WR-2.2 near field OEWG probe.

THz BSTA is shown in Fig. 8. A WR-2.2 open end wave guide (OEWG) probe was used to measure the near field amplitude and phase data, and NSI commercial software based on fast Fourier transform (FFT) algorithm was used to transform the near-field data to far-field radiation pattern. The gain comparison method is used to measure the gain of BSTA.

As the feed moving to 0 mm, ±3.06 mm, ±6.17 mm, and ±9.38 mm offsets the focal point, the main beams pointing to 0°, ±5°, ±10°, and ±15° are obtained. Computed and measured scanning radiation patterns of the THz BSTA in $H$-plane at 340 GHz are shown in Fig. 9. The measurement results are in very good agreement with the theoretical calculations. Fig. 10 shows the measured gain versus frequency curves for the broadside and OFF-axis beams. The measured broadside beam presents a peak gain of 39.5 dBi at 340 GHz, which implies an aperture and radiation efficiency of 10.5% and 70.8%, respectively, and a −3 dB gain bandwidth of 11.8%. Besides, the OFF-axis beam pointing to 15° presents a peak gain of 38.3 dBi and a −3 dB gain bandwidth of 10%.

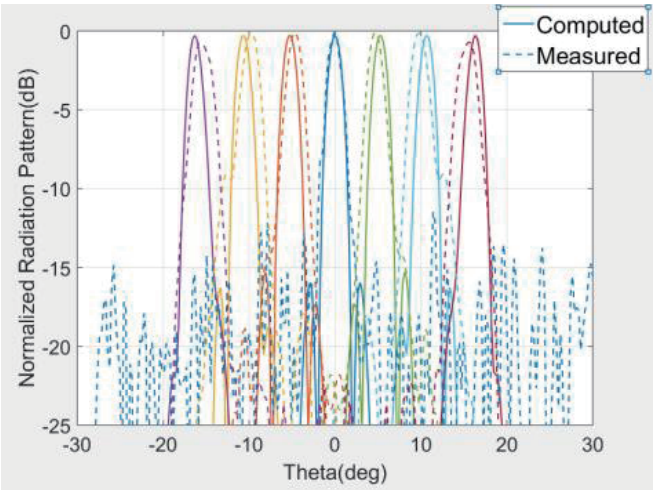


**Figure 9.** Computed and measured scanning radiation patterns of THz BSTA in $H$-plane at 340 GHz.

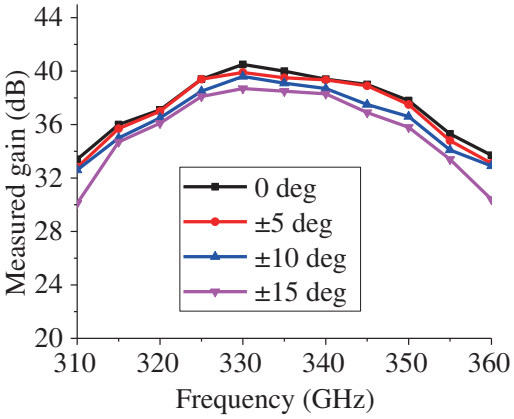


**Figure 10.** Measured gain versus frequency for the broadside and OFF-axis beams.

The measured performances of the THz BSTA are show in Table 1. The measured gain of scanning beams is superior to 38.3 dB at 340 GHz. Very low scanning loss of 1.2 dB with scanning range of $-15° \sim 15°$ is reached. The half power beam width (HPBW) of the scanning beams are less than 2°,

**Table 1.** The measured performances of THz BSTA.

| Beam pointing | Gain (dBi) | HPBW | SLL (dB) | −1 dB Gain BW | −3 dB Gain BW |
|---|---|---|---|---|---|
| 0° | 39.5 | 2° | −19.4 | 7.6% | 11.8% |
| ±5° | 39.35 | 1.93° | −18.8 | 6.7% | 11.2% |
| ±10° | 38.7 | 1.96° | −17.8 | 6.5% | 10.3% |
| ±15° | 38.3 | 1.98° | −25 | 6.5% | 10% |

and the side lobe level (SLL) is less than −17.8 dB for all scanning beams, which demonstrates that high performance scanning beams are radiated by the BSTA at terahertz band. The aperture efficiency, $AE$, is calculated by the following formulas [23]:

$$AE = \frac{G}{D_{\max}} \quad D_{\max} = \frac{4\pi A}{\lambda_0^2} \tag{6}$$

where $G$ is the measured gain, $D_{\max}$ the maximum directivity and $A$ the area of the antenna's aperture. The aperture efficiency of the broadside beam is calculated to be 10.5%.

The measured co- and cross-polarization radiation patterns of broadside beam at 320 GHz, 340 GHz, and 360 GHz are shown in Fig. 11 ($H$-plane and $E$-plane). The measured cross-polarization levels are

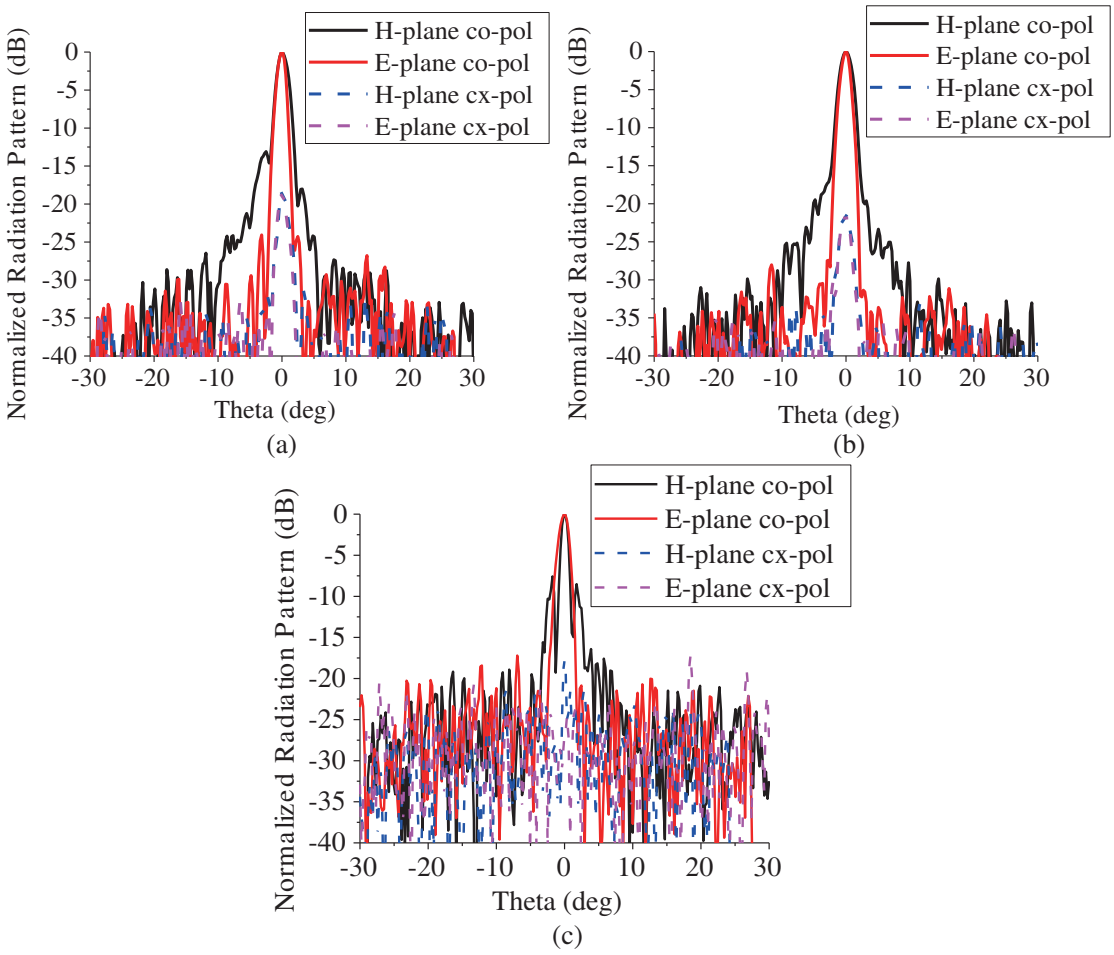


**Figure 11.** Measured co- and cross-polarization radiation patterns of broadside beam at (a) 320 GHz, (b) 340 GHz and (c) 360 GHz.

lower than −18.3 dB, −21.2 dB, and −18 dB at 320 GHz, 340 GHz, and 360 GHz, respectively. The measured side lobe levels in two principal planes are lower than −19.1 dB at center working frequency. It can be observed that the proposed prototype reaches excellent radiation performances above 300 GHz in terms of gain, aperture efficiency, side lobe level, and cross-polarization level. A brief comparison with other state-of-the-art THz TA prototypes (none beam steering TA working above 140 GHz found yet) using different techniques is given in Table 2. It can be seen that its aperture efficiency is not very ideal, but the working frequency, peak gain, scanning range, and loss of the proposed design are very attractive for beam steering application at THz band.

**Table 2.** Comparison with state-of-the-art THz transmitarrays.

| Ref. | [8] | [9] | [10] | [11] | [12] | [14] | This work |
|---|---|---|---|---|---|---|---|
| Freq. (GHz) | 250 | 300 | 300 | 140 | 145 | 300 | 340 |
| Polarization | LP | CP | LP | LP | LP | LP | LP |
| Technology | PCB | PCB | PCB | LTCC | PCB | PCB | MEMS |
| No. metal layers | 2 | 4 | 3 | 7 | 3 | 3 | 4 |
| Diameter | $14\lambda$ | $12.6\lambda$ | $16.5\lambda$ | $20\lambda$ | $20\lambda$ | $20\lambda$ | $101.1\lambda \times 79.5\lambda$ |
| Peak gain (dBi) | 28.8 | 26.3 | 28.7 | 33.5 | 33.0 | 32.2 | 39.5 |
| −1-dB Gain BW | 6.8% | — | 23% | 10.7% | 11.7% | 10.5% | 7.6% |
| Aperture efficiency | 32% | 21.4% | 31.2% | 50.1% | 38.3% | 36.5% | 10.5% |
| Scanning range | — | — | | — | — | — | 30° |
| Scanning loss | — | — | | — | — | — | 1.2 dB |

## 5. CONCLUSION

A terahertz high gain beam steering TA with low scan loss is demonstrated in the paper. To validate the scanning performance, a prototype is manufactured by micromachining process. The measured results show that the THz BSTA could realize beam scanning in a wide angular range of $-15^\circ \sim 15^\circ$ with scanning loss lower than 1.2 dB. High performances such as high gain ($> 38.3$ dB), comparative narrow beamwidth ($< 2^\circ$) and low side lobe level ($< -17.8$ dB) are also achieved by the scanning beams.

## ACKNOWLEDGMENT

The authors thank the National Space Science Center, CAS and National Natural Science Foundation of China under Grant 62171432 for the funding support.

## REFERENCES

1. Chattopadhyay, G., "Terahertz antennas and systems for space borne platforms," *Proc. 4th Eur. Conf. Antennas Propag.*, 1–7, Barcelona, 2010.
2. Liu, F., W. Z. Cui, Z. B. Zhu, S. W. Dong, S. Shang, and Z. S. Yao, "The spaceborne terahertz remote sensing techniques," *IET International Radar Conference 2013*, 1–5, Xi'an, 2013.
3. Read, W. G., Z. Shippony, M. J. Schwartz, and W. V. Snyder, "The clear-sky unpolarized forward model for the EOS aura microwave limb sounder (MLS)," *IEEE Trans. Geosci. Remote Sens.*, Vol. 44, No. 5, 1367–1379, May 2006.
4. Abdelrahman, A. H., F. Yang, A. Z. Elsherbeni, and P. Nayeri, "Analysis and design of transmitarray antennas," *Synthesis Lectures on Antennas*, Vol. 6, No. I, 1–175, 2017.

5. Kaouach, H., L. Dussopt, J. Lanteri, T. Koleck, and R. Sauleau, "Wideband low-loss linear and circular polarization transmit-arrays in V-band," *IEEE Trans. Antennas Propag.*, Vol. 59, No. 7, 2513–2523, Jul. 2011.
6. Pham, K. T., G. Liu, D. G. Ovejero, and R. Sauleau, "Dual-band transmitarray with low scan loss for satcom applications," *IEEE Trans. Antennas Propag.*, Vol. 69, No. 3, 1775–1780, Mar. 2021.
7. Qu, S. W., H. Yi, B. J. Chen, K. B. Ng, and C. H. Chan, "Terahertz reflecting and transmitting metasurfaces," *Proc. IEEE*, Vol. 105, No. 6, 1166–1184, Jun. 2017.
8. Qu, S. W. and H. Yi, "Low-cost two-layer terahertz transmitarray," *2017 International Applied Computational Electromagnetics Society Symposium (ACES)*, 1–2, Suzhou, 2017.
9. Yi, H., K. B. Ng, C. K. Wong, S. W. Qu, and C. H. Chan, "A low-cost satellite-to-satellite link using meta-lens," *12th Eur. Conf. Antennas Propag.*, London, UK, Apr. 9–13, 2018.
10. Qu, S. W., P.-Y. Feng, H. Yi, et al., "Terahertz reflectarray and transmitarray," *2016 International Symposium on Antennas and Propagation (ISAP)*, 548–549, Okinawa, Japan, 2016,
11. Miao, Z., Z.-C. Hao, G. Q. Luo, et al., "140 GHz high-gain LTCC-integrated transmit-array antenna using a wideband SIW aperture-coupling phase delay structure," *IEEE Trans. Antennas Propag.*, Vol. 66, No. 1, 182–190, Jan. 2018.
12. Foglia Manzillo, F., A. Clemente, and J. L. González-Jiménez, "High-gain D-band transmitarrays in standard PCB technology for beyond-5G communications," *IEEE Trans. Antennas Propag.*, Vol. 68, No. 1, 587–592, Jan. 2020.
13. Liu, G., H. Wang, J. Jiang, and F. Xue, "Terahertz substrateless transmitarray antenna design and microfabrication," *Microw. Opt. Technol. Lett.*, Vol. 58, No. 9, 2096–2100, Sep. 2016.
14. Koutsos, O., F. F. Manzillo, A. Clemente, and R. Sauleau, "Analysis, rigorous design, and characterization of a three-layer anisotropic transmitarray at 300 GHz," *IEEE Trans. Antennas Propag.*, Vol. 70, No. 7, 5437–5446, Jul. 2022
15. Pan, X., F. Yang, S. Xu, and M. Li, "Review of W-band reconfigurable reflectarray and transmitarray antennas at tsinghua university," *$14^{th}$ Eur. Conf. Antennas Propag.*, Copenhagen, Denmark, 2020.
16. Pan, X., S. Wang, G. Li, S. Xu, and F. Yang, "On-chip reconfigurable reflectarray for 2-D beam-steering at W-band," *2018 IEEE MTT-S International Wireless Symposium (IWS)*, 1–4, Chengdu, 2018,
17. Pham, K., N. T. Nguyen, A. Clemente, L. Di Palma, L. Le Coq, L. Dussopt, and R. Sauleau, "Design of wideband dual linearly-polarized transmitarray antennas," *IEEE Trans. Antennas Propag.*, Vol. 64, No. 5, 2022–2026, May 2016.
18. Lima, E. B., S. A. Matos, J. R. Costa, C. A. Fernandes, and N. J. G. Fonseca, "Circular polarization wide-angle beam steering at Ka-band by in-plane translation of a plate lens antenna," *IEEE Trans. Antennas Propag.*,Vol. 63, No. 12, 5443–5455, Dec. 2015.
19. Matos, S. A., E. B. Lima, J. R. Costa, C. A. Fernandes, and N. J. G. Fonseca, "Design of a 40 dBi planar bifocal lens for mechanical beam steering at Ka-band," *10th Eur. Conf. Antennas Propag.*, Davos, Switzerland, 2016.
20. Liu, G., Z. Wang, and H. Wang, "Low loss multi-beam terahertz transmitarray antenna for remote sensing," *2019 PhotonIcs & Electromagnetics Research Symposium — Fall (PIERS — FALL)*, 2873–2877, Xiamen, China, Dec. 17–20, 2019.
21. Liu, G., E. M. Cruz, K. Pham, D. G. Ovejero, and R. Sauleau, "Low scan loss bifocal Ka-band transparent transmitarray antenna," *IEEE Int. Symp. Antennas Propag. (APS/URSI)*, 1449–1450, Boston, MA, USA, 2018,
22. Heymann, M., S. Fraden, and D. Kim, "Multi-height precision alignment with selectively developed alignment marks," *Journal of Microelectromechanical Systems*, Vol. 23, No. 2, 424–427, Apr. 2014.
23. Abdelrahman, A. H., A. Z. Elsherbeni, and F. Yang, "High-gain and broadband transmitarray antenna using triple-layer spiral dipole elements," *IEEE Antennas Wireless Propag. Lett.*, Vol. 13, 2014.